



HAL
open science

Detecting, estimating and correcting multipath biases affecting GNSS signals using a marginalized likelihood ratio-based method

Cheng Cheng, Jean-Yves Tournet, Quan Pan, Vincent Calmettes

► **To cite this version:**

Cheng Cheng, Jean-Yves Tournet, Quan Pan, Vincent Calmettes. Detecting, estimating and correcting multipath biases affecting GNSS signals using a marginalized likelihood ratio-based method. *Signal Processing*, 2016, vol. 118, pp. 221-234. 10.1016/j.sigpro.2015.06.021 . hal-01260529

HAL Id: hal-01260529

<https://hal.science/hal-01260529v1>

Submitted on 22 Jan 2016

HAL is a multi-disciplinary open access archive for the deposit and dissemination of scientific research documents, whether they are published or not. The documents may come from teaching and research institutions in France or abroad, or from public or private research centers.

L'archive ouverte pluridisciplinaire **HAL**, est destinée au dépôt et à la diffusion de documents scientifiques de niveau recherche, publiés ou non, émanant des établissements d'enseignement et de recherche français ou étrangers, des laboratoires publics ou privés.



Open Archive TOULOUSE Archive Ouverte (OATAO)

OATAO is an open access repository that collects the work of Toulouse researchers and makes it freely available over the web where possible.

This is an author-deposited version published in : <http://oatao.univ-toulouse.fr/>
Eprints ID : 14692

To link to this article : DOI:10.1016/j.sigpro.2015.06.021
URL : <http://dx.doi.org/10.1016/j.sigpro.2015.06.021>

To cite this version :

Cheng, Cheng and Tourneret, Jean-Yves and Pan, Quan and Calmettes, Vincent *Detecting, estimating and correcting multipath biases affecting GNSS signals using a marginalized likelihood ratio-based method.* (2016) *Signal Processing*, vol. 118. pp. 221-234.
ISSN 0165-1684

Any correspondence concerning this service should be sent to the repository administrator: staff-oatao@listes-diff.inp-toulouse.fr

Detecting, estimating and correcting multipath biases affecting GNSS signals using a marginalized likelihood ratio-based method

Cheng Cheng^{a,b}, Jean-Yves Tourneret^{c,1}, Quan Pan^{a,*}, Vincent Calmettes^b

^a School of Automation, Northwestern Polytechnical University, Xi'an, China

^b SCANR/DEOS-ISAE, University of Toulouse, Toulouse, France

^c IRIT/INP-ENSEEIH, University of Toulouse, Toulouse, France

A B S T R A C T

In urban canyons, non-line-of-sight (NLOS) multipath interferences affect position estimation based on global navigation satellite systems (GNSS). This paper proposes to model the effects of NLOS multipath interferences as mean value jumps contaminating the GNSS pseudo-range measurements. The marginalized likelihood ratio test (MLRT) is then investigated to detect, identify and estimate the corresponding NLOS multipath biases. However, the MLRT test statistics is difficult to compute. In this work, we consider a Monte Carlo integration technique based on bias magnitude sampling. Jensen's inequality allows this Monte Carlo integration to be simplified. The multiple model algorithm is also used to update the prior information for each bias magnitude sample. Some strategies are designed for estimating and correcting the NLOS multipath biases. In order to demonstrate the performance of the MLRT, experiments allowing several localization methods to be compared are performed. Finally, results from a measurement campaign conducted in an urban canyon are presented in order to evaluate the performance of the proposed algorithm in a representative environment.

Keywords:

Global navigation satellite systems
Multipath mitigation
Marginalized likelihood ratio test
Multiple model
Urban positioning

1. Introduction

Global navigation satellite systems (GNSS) have been widely used in many applications requiring demanding signal processing algorithms. These applications include surveillance of unmanned aerial/landing vehicles, search and rescue in urban canyons and location-based intelligent transport system applications. In these applications, the multipath (MP) interference is one of the largest sources of GNSS errors. MP errors are mainly due to the fact that a

signal transmitted by a satellite is very likely to be reflected or diffracted and can follow different paths before arriving at the GNSS receiver antenna [1]. MP interferences can be divided into two classes: (a) the non-line-of-sight (NLOS) interferences which result from a unique reflected signal received and tracked by the GNSS receiver; (b) the line-of-sight (LOS) interferences which result from the sum of the direct signal and of delayed reflections. NLOS interferences frequently occur in urban canyons, where the direct path of a satellite signal is vulnerable to masking or blocking whereas reflected signals can be tracked within the receiver [2].

Different approaches can be found in the literature for mitigating MP interference errors. The use of high quality antenna arrays has shown to be efficient for detecting and mitigating MP [3,4], or for estimating parameters of MP

* Corresponding author.

E-mail addresses: cheng.cheng@isae.fr (C. Cheng),
jean-yves.tourneret@enseeiht.fr (J.-Y. Tourneret),
quanpan@nwpu.edu.cn (Q. Pan), vincent.calmettes@isae.fr (V. Calmettes).

¹ EURASIP member.

components. Unfortunately, these antennas are expensive and have large dimensions. Considering that the GNSS receiver has to track the signal composed of the direct signal and of delayed reflections in the LOS situation, several MP mitigation methods based on the narrow correlator delay lock loop [5] have been proposed, such as the strobe correlator [6], the early-late-slope technique [7], the double-delta correlator [8] and the MP insensitive delay lock loop [9]. Moreover, the direct and reflected signal parameters can be estimated by using a robust statistical approach based on maximum likelihood principle [10–14]. Bayesian approaches have also been proposed to estimate the MP parameters within GNSS receivers since they allow the nonlinear estimation problem to be handled [15–18]. In the NLOS situation, MP interferences can be hardly mitigated by these strategies while the direct signal is blocked or masked. To overcome these difficulties, a 3D model of the environment can be used to deliver a priori knowledge about the shadowed satellites [19,20]. Another possibility is to exploit the geometric path model [21] in order to estimate a possible reflected path related to NLOS MP interferences. The reflected signal due to an MP interference can be converted to a bias appearing on the GNSS pseudo-range measurement. When prior information for this bias is obtained, MP mitigation methods based on Bayesian statistical theory can be considered [22]. For instance, Spangenberg considered in [23] two different models for pseudo-range measurements depending on the availability of LOS signals. Viandier proposed in [24] different ways of handling pseudo-range measurements contaminated by MP biases in urban scenarios, and of estimating the position of a vehicle by using a particle filter applied to a jump Markov system. Giremus proposed in [25] a fixed Rao-blackwellized particle filter to jointly detect and estimate MP biases associated with GNSS pseudo-range measurements.

The generalized likelihood ratio test (GLRT) (also known as the Bayesian detector [26]), used for fault detection and diagnosis in a state space was first proposed by Willsky and Jones [27]. In this GLRT, the test statistic is the innovation sequence of the Kalman filter and nuisance parameters appearing in the test statistic are replaced by their maximum likelihood estimator. The marginalized likelihood ratio test (MLRT) proposed by Gustafsson [28] incorporates prior knowledge about the nuisance parameters that are eliminated by the marginalization of the likelihood function. Accordingly, different bias detection and isolation approaches have been developed based on the MLRT. For instance, dos Santos proposed in [29] a maximum a posteriori criterion based on the marginalization of the likelihood function with the gamma prior distribution. Kiasi proposed in [30] a modified MLRT with a uniform distribution to estimate the occurrence time of fault. Considering that the test statistic of the MLRT is generally difficult to compute, Giremus proposed in [31] a numerical solution based on the unscented transform to solve this problem.

In this work, we propose an approximated marginalized likelihood ratio test based on Jensen's inequality to detect, identify and estimate the NLOS multipath biases affecting GNSS pseudo-range measurements. The test

statistic in the MLRT is approximated by a Monte Carlo integration technique based on bias magnitude sampling. Jensen's inequality allows this Monte Carlo integration to be simplified, and the multiple model algorithm is used to update the prior information for each bias magnitude sample. Some strategies are also designed for estimating and correcting the NLOS multipath biases. The empirical cumulative distribution function of the approximate test statistic is analyzed and the corresponding detection threshold is determined via Monte Carlo simulations. In addition, a comprehensive simulation study is implemented to compare the performance of the proposed approach with other state-of-the-art detection approaches. Finally, the proposed approach is evaluated based on data obtained from a measurement campaign conducted in a street urban canyon.

The paper is organized as follows: the system considered for GNSS positioning is introduced in Section 2. Section 3 studies the MLRT and its approximation based on Jensen's inequality to detect MP biases possibly affecting GNSS measurements. Section 4 investigates the identification, estimation and correction of GNSS measurements in the presence of NLOS MP biases. Section 5 analyzes the test statistic used in the proposed MP detection approach. The performance of the proposed algorithm is evaluated in Section 6, first from simulated data representative of realistic scenarios, and then from real data collected by a UBLOX receiver operating in an urban canyon. Conclusions are finally reported in Section 7.

2. System description

2.1. State model

For the considered application which addresses vehicles moving slowly in an urban environment, we investigate a second-order model (i.e., a constant velocity model) to describe the dynamic of the vehicle in the earth-centered earth-fixed (ECEF) frame. Moreover, the GNSS receiver clock offset and its drift are taken into account. Therefore, the state model can be divided into two parts containing the position and velocity of the vehicle in the ECEF frame, and the receiver clock offset and drift, respectively. More precisely, the state vector considered in this paper is defined as follows [32]:

$$\mathbf{X}_t = (x_t, \dot{x}_t, y_t, \dot{y}_t, z_t, \dot{z}_t, b_t, d_t)^\top \quad (1)$$

where (x_t, y_t, z_t) and $(\dot{x}_t, \dot{y}_t, \dot{z}_t)$ are the vehicle position and velocity in the ECEF frame (Cartesian coordinate), respectively, b_t and d_t are the GNSS receiver clock offset and drift, $(\cdot)^\top$ is the transpose of a vector.

The velocity can be reasonably modelled as a random walk, e.g., $\ddot{x} = e_x$ where e_x is a zero mean Gaussian noise of variance σ_a^2 . For short-term applications in which the periodical clock resets of the GNSS receiver are not taken into account, the GNSS receiver clock offset b_t and its drift d_t can also be modelled as random walks, i.e., $\dot{b}_t = d_t + e_b$ and $\dot{d}_t = e_d$ where e_b and e_d are zero-mean Gaussian white noises of variance σ_b^2 and σ_d^2 . Based on the above assumptions, the discrete-time state model which describes the

propagation of the vehicle state \mathbf{X}_t can be formulated as

$$\mathbf{X}_{k+1} = \Phi_{k+1|k} \mathbf{X}_k + \mathbf{e}_k \quad (2)$$

where $k = 1, \dots, K$ denotes the k th sampling time instant, $\mathbf{e}_k = (e_x, e_y, e_z, e_b, e_d)^T$ is the zero mean Gaussian white noise vector of covariance matrix \mathbf{Q}_k . Considering a relative independence between the kinematic parameters and the GNSS clock parameters, the state matrix $\Phi_{k+1|k}$ is a block-diagonal matrix. More precisely, the matrices $\Phi_{k+1|k}$ and \mathbf{Q}_k can be defined as follows:

$$\Phi_{k+1|k} = \begin{pmatrix} \mathbf{A}_k & \mathbf{0} \\ \mathbf{0} & \mathbf{C}_k \end{pmatrix} \quad \text{and} \quad \mathbf{Q}_k = \begin{pmatrix} \Sigma_k^a & \mathbf{0} \\ \mathbf{0} & \Sigma_k^c \end{pmatrix} \quad (3)$$

where the block matrices \mathbf{A}_k , \mathbf{C}_k , Σ_k^a and Σ_k^c are

$$\mathbf{A}_k = \begin{pmatrix} \mathbf{C}_k & \mathbf{0} & \mathbf{0} \\ \mathbf{0} & \mathbf{C}_k & \mathbf{0} \\ \mathbf{0} & \mathbf{0} & \mathbf{C}_k \end{pmatrix}, \quad \mathbf{C}_k = \begin{pmatrix} 1 & \Delta t \\ 0 & 1 \end{pmatrix} \quad (4)$$

$$\Sigma_k^a = \begin{pmatrix} \mathbf{Q}_k^a & \mathbf{0} & \mathbf{0} \\ \mathbf{0} & \mathbf{Q}_k^a & \mathbf{0} \\ \mathbf{0} & \mathbf{0} & \mathbf{Q}_k^a \end{pmatrix}, \quad \mathbf{Q}_k^a = \sigma_a^2 \begin{pmatrix} \frac{\Delta t^4}{4} & \frac{\Delta t^3}{2} \\ \frac{\Delta t^3}{2} & \Delta t^2 \end{pmatrix} \quad (5)$$

$$\Sigma_k^c = \begin{pmatrix} \sigma_b^2 \Delta t^2 + \sigma_d^2 \frac{\Delta t^4}{4} & \sigma_d^2 \frac{\Delta t^3}{2} \\ \sigma_d^2 \frac{\Delta t^3}{2} & \sigma_d^2 \Delta t^2 \end{pmatrix} \quad (6)$$

and where Δt represents the time interval between two successive sampling instants.

2.2. Measurement model in the presence of multipath

As the GNSS receiver tracking loops filter MP interferences whose relative delays vary with time, only the MP interferences resulting in a constant bias affecting the pseudo-range measurements (during the observation period) are considered in this paper. Thus we introduce a mean value jump affecting the GNSS pseudo-range measurements in the presence of NLOS MP interferences. Consequently, the m th in-view satellite pseudo-range measurement model including an NLOS MP bias can be defined as [32]

$$Z_k^m = \sqrt{(x_k^m - x_k)^2 + (y_k^m - y_k)^2 + (z_k^m - z_k)^2} + b_k + v_{k,\theta}^m + e_k^m \quad (7)$$

where Z_k^m ($m = 1, \dots, N_s$) is the pseudo-range measurement associated with the m th in-view satellite, N_s is the number of in-view satellites, (x_k^m, y_k^m, z_k^m) and (x_k, y_k, z_k) are the m th satellite position and the vehicle position in the ECEF frame, respectively, b_k is the GNSS receiver clock offset, $v_{k,\theta}^m$ is the magnitude of the NLOS MP bias associated with the m th pseudo-range measurement, characterized by the parameter θ which represents the possible occurrence time of the NLOS MP bias ($\theta = k$ for $v=0$), and e_k^m is the m th satellite pseudo-range measurement noise with a normal distribution $e_k^m \sim \mathcal{N}(0, \sigma_r^2)$ where $\mathcal{N}(\cdot)$ is a univariate Gaussian distribution with mean value 0 and variance σ_r^2 .

In (7), the pseudo-range measurement related to the vehicle position is defined by a non-linear equation of the vehicle position. An unscented Kalman filter and a particle filter could be investigated with the advantage to estimate

the state of this non-linear estimation problem. However, the corresponding computational costs of these filters can be prohibitive for practical applications. Thus, we consider in this chapter an extended Kalman filter (EKF) which leads to apply a conventional Kalman filter by linearizing the non-linear equation (7) and is known to provide an efficient and low-cost solution for weakly non-linear systems.

3. Non-line-of-sight bias detection based on MLRT

3.1. Problem formulation

In the NLOS situation, we propose to model the MP interference as a mean value jump affecting the GNSS pseudo-range measurements. We assume that NLOS MP biases do not appear simultaneously on different pseudo-range measurements and that the pseudo-range measurement which is affected by NLOS MP bias is known. The case of multiple NLOS MP interferences appearing simultaneously on different pseudo-range measurements will be discussed in the next section. Assuming that only the m th satellite measurement is contaminated, the NLOS MP bias vector for the pseudo-range measurements is denoted as $\mathbf{v} = (0, \dots, v, \dots, 0) \in \mathbb{R}^{N_s}$ where the only non-zero element of \mathbf{v} is located at the known position m .

According to the hypothesis testing theory, the likelihood ratio test for detecting the presence or absence of a mean value jump is a binary hypothesis test which compares two likelihood functions associated with the absence (H_0) and presence (H_1) of a mean value jump in the measurements. The two hypotheses considered in this paper are defined as follows:

H_0 : no mean value jump up to present time k ,

H_1 : a mean value jump (of amplitude $v \neq 0$)

has occurred at time $\theta < k$.

The log-likelihood ratio for these two hypotheses is

$$l_k(\theta, v) = \ln \frac{p(\mathbf{Z}_{1:k} | H_1(\theta, v))}{p(\mathbf{Z}_{1:k} | H_0)} \quad (8)$$

where $\mathbf{Z}_{1:k} = \{\mathbf{Z}_i\}_{i=1}^k$ is the pseudo-range measurement vector sequence up to time k with $\mathbf{Z}_i = (Z_i^1, \dots, Z_i^{N_s})^T$, and N_s is the number of in-view satellites. Note that we have denoted as $p(\mathbf{Z}_{1:k} | H_1(\theta, v))$ and $p(\mathbf{Z}_{1:k} | H_0)$ the probability density functions of the measurement vector associated with the hypotheses H_1 and H_0 respectively.

In the likelihood ratio test, the occurrence time and the magnitude of the mean value jump denoted as θ and v are assumed to be known. However, in practice the jump magnitude v is unknown and can be regarded as a nuisance parameter for the likelihood ratio test. According to the literature, there are two classes of methods for eliminating the nuisance parameter v . The first method consists of replacing the nuisance parameter by its maximum likelihood estimator (maximizing the likelihood function) in the probability density function $p(\mathbf{Z}_{1:k} | H_1(\theta, v))$ leading to the GLRT. The second method marginalizes the log-likelihood ratio with respect to the nuisance parameter yielding the MLRT. The key point of the GLRT based on a state space model is that the

maximum likelihood estimator of parameter ν can be obtained by the innovation of an appropriate Kalman filter. Contrary to the GLRT, the nuisance parameter ν is eliminated by marginalization of the likelihood function under the hypothesis H_1 in the MLRT. In [28], Gustafsson proposed an MLRT approach based on a state space model as a more robust method for bias detection. Unfortunately, the marginal likelihood function under hypothesis H_1 is generally difficult to compute in the MLRT. An alternative was proposed by Giremus in [31] where a numerical solution of the MLRT based on the unscented transform was used for bias detection in space state models. The method studied in [31] introduced a prior distribution for the nuisance parameter ν which can be obtained from our experience about MP or from previous experiments. This work studies a similar approach which differs from [31] by the use of an approximation based on Jensen's inequality, as explained below. According to the error envelope of MP interferences (which is a function of the MP relative delay interfering the direct signal for a given GNSS receiver configuration [33]), a possible prior distribution for the MP bias with magnitude ν is a uniform distribution defined by $p(\nu) \sim U(\nu_{\min}, \nu_{\max})$ where $U(\cdot)$ denotes the uniform distribution, ν_{\min} and ν_{\max} are the minimum and maximum magnitudes of the MP bias, respectively. This distribution reflects the fact that the only knowledge about MP biases is their minimum and maximum values that have to be specified by the user, depending on the environment. Using this prior distribution for the nuisance parameter, we propose in this paper an approximate MLRT based on Jensen's inequality to detect the occurrence time of NLOS MP biases.

The marginalization of (8) with respect to ν leads to

$$l_k(\theta) = \ln \frac{p(\mathbf{Z}_{1:k}|\mathbf{H}_1(\theta))}{p(\mathbf{Z}_{1:k}|\mathbf{H}_0)} \quad (9)$$

where

$$p(\mathbf{Z}_{1:k}|\mathbf{H}_1(\theta)) = \int p(\mathbf{Z}_{1:k}|\mathbf{H}_1(\theta, \nu))p(\nu) d\nu \quad (10)$$

and where $p(\nu)$ is the prior distribution of ν . Considering that the integral in (10) is difficult to compute in closed-form, a Monte Carlo integration method can be used to evaluate (10). According to the Monte Carlo integration, (10) is approximated as

$$p(\mathbf{Z}_{1:k}|\mathbf{H}_1(\theta)) \approx \sum_{i=1}^n \omega^i p(\mathbf{Z}_{1:k}|\mathbf{H}_1(\theta, \nu_i)) \quad (11)$$

where ν_i ($i = 1, \dots, n$) is the i th sampling value of the MP bias magnitude belonging to the interval (ν_{\min}, ν_{\max}) , and n is the number of magnitude samples. Accordingly, a group of NLOS MP bias vectors (denoted as $\mathbf{v}_i = (0, \dots, \nu_i, \dots, 0)$ for $i = 1, \dots, n$) are generated with weights $\omega^i = 1/n$ such that $\sum_{i=1}^n \omega^i = 1$. As a consequence, the test statistic $l_k(\theta)$ in the MLRT can be approximated as

$$l_k(\theta) = \ln \frac{p(\mathbf{Z}_{1:k}|\mathbf{H}_1(\theta))}{p(\mathbf{Z}_{1:k}|\mathbf{H}_0)} \approx \ln \frac{\sum_{i=1}^n \omega^i p(\mathbf{Z}_{1:k}|\mathbf{H}_1(\theta, \nu_i))}{p(\mathbf{Z}_{1:k}|\mathbf{H}_0)} \quad (12)$$

By decomposing the pseudo-range measurement vector sequence as $\mathbf{Z}_{1:k} = \{\mathbf{Z}_{1:\theta-1}, \mathbf{Z}_{\theta:k}\}$, the probability density

functions of the measurement vector associated with the hypotheses H_1 and H_0 can be rewritten as

$$\begin{aligned} p(\mathbf{Z}_{1:k}|\mathbf{H}_1(\theta, \nu)) &= p(\mathbf{Z}_{\theta:k}|\mathbf{Z}_{1:\theta-1}, \mathbf{H}_1(\theta, \nu))p(\mathbf{Z}_{1:\theta-1}|\mathbf{H}_1(\theta, \nu)) \\ p(\mathbf{Z}_{1:k}|\mathbf{H}_0) &= p(\mathbf{Z}_{\theta:k}|\mathbf{Z}_{1:\theta-1}, \mathbf{H}_0)p(\mathbf{Z}_{1:\theta-1}|\mathbf{H}_0). \end{aligned} \quad (13)$$

Since $\nu = 0$ for $k < \theta$, using (13) in (12) leads to

$$l_k(\theta) = \ln \frac{\sum_{i=1}^n \omega^i p(\mathbf{Z}_{\theta:k}|\mathbf{Z}_{1:\theta-1}, \mathbf{H}_1(\theta, \nu_i))}{p(\mathbf{Z}_{\theta:k}|\mathbf{Z}_{1:\theta-1}, \mathbf{H}_0)}. \quad (14)$$

The maximum likelihood estimator of the occurrence time θ is

$$\hat{\theta} = \underset{\theta}{\operatorname{argmax}} l_k(\theta). \quad (15)$$

The presence of a mean value jump is decided using the following MLRT rule:

$$l_k(\hat{\theta}) \underset{H_0}{\overset{H_1}{\geq}} \varepsilon \quad (16)$$

where ε is a threshold related to the probability of false alarm of the test. In order to reduce the computational complexity, the optimization of θ is constrained to the last L_w units of time, i.e., $k - L_w < \theta \leq k$ at any time k , where L_w is the window length.

3.2. An approximate MLRT based on Jensen's inequality

According to the Kalman filter theory, the denominator of (14) which is the likelihood function associated with the hypothesis H_0 can be defined as

$$p(\mathbf{Z}_{\theta:k}|\mathbf{Z}_{1:\theta-1}, \mathbf{H}_0) = \prod_{j=\theta}^k p(\mathbf{Z}_j|\mathbf{Z}_{1:j-1}, \mathbf{H}_0) \quad (17)$$

with

$$p(\mathbf{Z}_j|\mathbf{Z}_{1:j-1}, \mathbf{H}_0) = \mathcal{N}(\mathbf{Z}_j; \hat{\mathbf{Z}}_{jj-1}^0, \mathbf{S}_j^0) = p(\mathcal{Y}_j^0|\mathbf{H}_0)$$

where $\mathcal{N}(\mathbf{Z}_j; \hat{\mathbf{Z}}_{jj-1}^0, \mathbf{S}_j^0)$ is a Gaussian distribution with mean vector $\hat{\mathbf{Z}}_{jj-1}^0$ and covariance matrix \mathbf{S}_j^0 , $\mathcal{Y}_j^0 = \mathbf{Z}_j - \hat{\mathbf{Z}}_{jj-1}^0$ and \mathbf{S}_j^0 are the filter innovation vector and covariance matrix under the hypothesis H_0 at time j , \mathbf{Z}_j and $\hat{\mathbf{Z}}_{jj-1}^0$ are the pseudo-range measurement and predicted measurement vectors under the hypothesis H_0 at time j , respectively. Thus, the numerator of (14) is a weighted sum of likelihood functions associated with different mean value jump hypotheses with magnitudes ν_i ($i = 1, \dots, n$). Indeed the likelihood function under the hypothesis of a mean value jump with magnitude ν_i is

$$p(\mathbf{Z}_{\theta:k}|\mathbf{Z}_{1:\theta-1}, \mathbf{H}_1(\theta, \nu_i)) = \prod_{j=\theta}^k p(\mathbf{Z}_j|\mathbf{Z}_{1:j-1}, \mathbf{H}_1(\theta, \nu_i)) \quad (18)$$

with

$$p(\mathbf{Z}_j|\mathbf{Z}_{1:j-1}, \mathbf{H}_1(\theta, \nu_i)) = \mathcal{N}(\mathbf{Z}_j; \hat{\mathbf{Z}}_{jj-1}^i, \mathbf{S}_j^i) = p(\tilde{\mathcal{Y}}_j^i|\mathbf{H}_1(\theta, \nu_i))$$

where $\tilde{\mathcal{Y}}_j^i = \mathcal{Y}_j^0 - \mathbf{v}_i$ and \mathbf{S}_j^i are the filter innovation vector and its associated covariance matrix, respectively, under the hypothesis H_1 with a bias magnitude ν_i at time j . Note that $\hat{\mathbf{Z}}_{jj-1}^i$ is the predicted measurement vector under the hypothesis H_1 with a bias magnitude ν_i at time j .

After replacing (17) and (18) in (14), the MLRT test statistic based on the Monte Carlo integration can be expressed as follows:

$$l_k(\theta) = \ln \frac{\sum_{i=1}^n \omega^i \prod_{j=\theta}^k \mathcal{N}(\mathbf{Z}_j; \hat{\mathbf{Z}}_{j|j-1}^i, \mathbf{S}_j^i)}{\prod_{j=\theta}^k \mathcal{N}(\mathbf{Z}_j; \hat{\mathbf{Z}}_{j|j-1}^0, \mathbf{S}_j^0)} \\ = \ln \frac{\sum_{i=1}^n \omega^i \prod_{j=\theta}^k p(\tilde{\gamma}_j^i | \mathbf{H}_1(\theta, v_i))}{\prod_{j=\theta}^k p(\gamma_j^0 | \mathbf{H}_0)}. \quad (19)$$

According to (19), it is clear that the multiplication of several normal probability density functions in the denominator can be easily handled by the logarithm function. Conversely, the numerator of (19) is a weighted sum of normal probability density functions and thus is not easily tractable after the logarithm operation. Since the natural logarithm is a concave function over its range, Jensen's inequality [34] can be advocated leading to

$$\ln \left[\sum_{i=1}^n \lambda_i g(x_i) \right] \geq \sum_{i=1}^n \lambda_i \ln g(x_i) \quad (20)$$

where $g(\cdot)$ is any functional, $\lambda_i > 0$ and $\sum_{i=1}^n \lambda_i = 1$. Expanding the numerator of (19), (20) leads to

$$\ln \sum_{i=1}^n \omega^i \prod_{j=\theta}^k p(\tilde{\gamma}_j^i | \mathbf{H}_1(\theta, v_i)) \geq \sum_{i=1}^n \omega^i \ln \prod_{j=\theta}^k p(\tilde{\gamma}_j^i | \mathbf{H}_1(\theta, v_i)). \quad (21)$$

After replacing (21) in (19), the test statistic $l_k(\theta)$ can be rewritten as follows:

$$l_k(\theta) = \ln \frac{\sum_{i=1}^n \omega^i \prod_{j=\theta}^k p(\tilde{\gamma}_j^i | \mathbf{H}_1(\theta, v_i))}{\prod_{j=\theta}^k p(\gamma_j^0 | \mathbf{H}_0)} \\ \geq \sum_{i=1}^n \omega^i \ln \prod_{j=\theta}^k p(\tilde{\gamma}_j^i | \mathbf{H}_1(\theta, v_i)) - \ln \prod_{j=\theta}^k p(\gamma_j^0 | \mathbf{H}_0) \triangleq \frac{1}{2} \tilde{l}_k(\theta), \quad (22)$$

i.e.,

$$\tilde{l}_k(\theta) = \left[\sum_{j=\theta}^k (\gamma_j^0)^T (\mathbf{S}_j^0)^{-1} (\gamma_j^0) - \sum_{i=1}^n \omega^i \sum_{j=\theta}^k (\tilde{\gamma}_j^i)^T (\mathbf{S}_j^i)^{-1} (\tilde{\gamma}_j^i) \right] + K' \quad (23)$$

where

$$K' = \sum_{j=\theta}^k \ln |\mathbf{S}_j^0| - \sum_{i=1}^n \omega^i \sum_{j=\theta}^k \ln |\mathbf{S}_j^i|$$

is independent of the measurements. According to (23), in order to obtain filter innovations based on n measurement equations, several measurement equations (as many measurement equations as the number of bias magnitude samples) have to be processed in parallel and the contributions of all these measurement equations are weighted by ω^i . In such case, each sample v_i corresponds to one measurement equation, and the weight of each measurement equation actually depends on how close the magnitude sample v_i is to the exact magnitude v . Thus, the weight associated with each measurement equation is time-varying (hidden Markov chain) and will be denoted

as $\tilde{\omega}_j^i$ (weight of the i th measurement equation at time j). After replacing ω^i by $\tilde{\omega}_j^i$ in (23), the following result can be obtained:

$$\tilde{l}_k(\theta) = \sum_{j=\theta}^k \left[(\gamma_j^0)^T (\mathbf{S}_j^0)^{-1} (\gamma_j^0) - \sum_{i=1}^n \tilde{\omega}_j^i (\tilde{\gamma}_j^i)^T (\mathbf{S}_j^i)^{-1} (\tilde{\gamma}_j^i) \right] + K \quad (24)$$

where

$$K = \sum_{j=\theta}^k \left[\ln |\mathbf{S}_j^0| - \sum_{i=1}^n \tilde{\omega}_j^i \ln |\mathbf{S}_j^i| \right].$$

Finally, using the previous derivations, the presence of a mean value jump is accepted or rejected using the following rule:

$$\tilde{l}_k(\theta) \underset{\mathbf{H}_0}{\overset{\mathbf{H}_1}{\geq}} \epsilon' \quad (25)$$

where ϵ' is a threshold related to the probability of false alarm of the test. The parameter θ is then replaced by its maximum likelihood estimator $\hat{\theta}$ defined as

$$\hat{\theta} = \underset{\theta}{\operatorname{argmax}} \tilde{l}_k(\theta). \quad (26)$$

The rest of this section discusses how to adjust the weights $\tilde{\omega}_j^i$ defining $\tilde{l}_k(\theta)$. Considering that several measurement equations need to be processed in parallel, $\tilde{\omega}_j^i$ can be computed based on the multiple model algorithm which is defined in [35]. A set of measurement models associated with the jump magnitude samples v_i ($i=1, \dots, n$) is denoted as

$$\mathbf{M} \triangleq \left\{ M^i \right\}_{i=1}^n \quad (27)$$

where $M^i = (0, \dots, v_i, \dots, 0)$ and the corresponding model probability $\tilde{\omega}_j^i$ can be obtained based on the current measurement \mathbf{Z}_j and the predicted model probability, leading to

$$\tilde{\omega}_j^i = p(M_j^i | \mathbf{Z}_j) \\ = \frac{1}{c} p(\tilde{\gamma}_j^i | \mathbf{H}_1(\theta, v_i)) p(M_j^i | \mathbf{Z}_{j-1}) \quad (28)$$

where $j = \theta, \dots, k$ and c is the normalization constant.

4. Identification/estimation/correction of multipath biases

According to the test statistic $\tilde{l}_k(\theta)$ resulting from the approximate MLRT derived in Section 3, the occurrence time of the NLOS MP bias can be estimated. In order to determine which pseudo-range measurements are affected by NLOS MP biases, we study in this section a simultaneous detection and identification procedure which allows NLOS MP biases appearing simultaneously on different pseudo-range measurements to be handled. Note that the pseudo-range measurements associated with a mean value jump can be isolated after the presence of an MP interference has been confirmed by the bias detection methods, such as the receiver autonomous

integrity monitoring (RAIM) method [32] and the method of [31]. However, considering that the number of in-view satellites is limited in urban scenarios, the exclusion of pseudo-range measurements may weaken the observability and impair the accuracy of positioning solution based on GNSS. In order to implement the positioning solution with a maximum of pseudo-range measurements, we propose in this paper to estimate the NLOS MP biases for correcting measurement errors related to these biases. All these operations referred to as identification, estimation and correction are detailed below.

4.1. Identification of multipath biases

In order to make identification possible, a possible method is to compute one MLRT test statistic for each in-view satellite pseudo-range measurement. In this case, two hypotheses for detecting the presence of an NLOS MP bias on the m th ($m = 1, \dots, N_s$) in-view satellite pseudo-range measurement can be defined as

- H_0^m : no mean value jump for the m th measurement up to present time k ,
- H_1^m : a mean value jump (of amplitude $v^m \neq 0$) has occurred for the m th measurement at time $\theta < k$.

The detection and identification of NLOS MP biases can be converted into a group of hypothesis tests for all pseudo-range measurements. The corresponding test statistic $\tilde{l}_k^m(\theta)$ ($m = 1, \dots, N_s$) associated with the hypothesis of an NLOS MP bias affecting the m th in-view satellite pseudo-range measurement from time θ to k can be obtained based on the approximate MLRT theory presented in Section 3. The maximum likelihood estimator of the occurrence time θ associated with the m th measurement is finally defined as

$$\hat{\theta}^m = \operatorname{argmax}_{\theta} \tilde{l}_k^m(\theta). \quad (29)$$

For detecting the presence of an NLOS MP bias at a possible occurrence time $\hat{\theta}^m$, our decision rule is

$$\tilde{l}_k^m(\hat{\theta}^m) \underset{H_0^m}{\overset{H_1^m}{\geq}} \varepsilon' \quad (30)$$

where ε' is the m th hypothesis threshold related to a given probability of false alarm. In order to simplify the computation, a set of possible amplitudes (for the NLOS MP biases) v_i ($i = 1, \dots, n$) can be uniformly sampled in the interval (v_{\min}, v_{\max}) , and used for each calculation of the test statistic $\tilde{l}_k^m(\theta)$.

4.2. Estimation and correction of multipath biases

The optimization of $\hat{\theta}$ is constrained to the data belonging to a finite window ($k - L_w < \hat{\theta} \leq k$). Since the bias detection has to be performed in real time, the value of L_w is set to a relatively small value, i.e., $L_w = 11$ in [27] or $L_w = 5$ in [28]. Note that a larger threshold could be chosen to control the probability of false alarm.

After it has been detected that the m th satellite pseudo-range measurement is affected by an NLOS MP

interference, we propose to estimate the magnitude of the NLOS MP bias. The multiple model algorithm is used to update the measurement model probabilities associated with the magnitude samples defining the proposed approximate MLRT. Thus the model probability $\tilde{\omega}_j^i$ depends on how close the magnitude sample v_i is to the exact magnitude v and can adaptively adjust for each magnitude sample v_i ($i = 1, \dots, n$). The bias magnitude estimation $\hat{v}^m(\hat{\theta}_k^m)$ for the m th in-view satellite pseudo-range measurement at time k can be defined as

$$\hat{v}^m(\hat{\theta}_k^m) = v_{\hat{i}_k} + \hat{r}_{\hat{i}_k}^m(\hat{\theta}_k^m) \quad (31)$$

with

$$\hat{i}_k = \operatorname{argmax}_i \tilde{\omega}_k^i \quad (32)$$

and

$$\hat{r}_{\hat{i}_k}^m(\hat{\theta}_k^m) = \frac{1}{k - \hat{\theta}_k^m + 1} \sum_{j=\hat{\theta}_k^m}^k \tilde{\gamma}_{\hat{i}_k j}^m \quad (33)$$

where n is the number of bias magnitude samples, $\hat{\theta}_k^m$ is the maximum likelihood estimator of the occurrence time θ associated with the m th measurement at time k , $v_{\hat{i}_k}$ is the \hat{i}_k th sampling value of the NLOS MP bias magnitude, $\tilde{\gamma}_{\hat{i}_k j}^m = Z_j^m - \hat{Z}_{\hat{i}_k j | j-1}^m$ is the filter innovation under the hypothesis H_1^m with a bias sampling magnitude $v_{\hat{i}_k}$, Z_j^m and $\hat{Z}_{\hat{i}_k j | j-1}^m$ are the m th in-view satellite pseudo-range and predicted pseudo-range measurements under the hypothesis H_1^m with a bias sampling magnitude $v_{\hat{i}_k}$ at time j , respectively.

Once the NLOS MP bias and its magnitude have been detected and estimated, we propose to correct the corresponding filter innovation and to use it for the positioning solution based on the standard EKF algorithm. For the m th pseudo-range measurement which is affected by the NLOS MP bias, the corresponding filter innovation can be corrected as follows:

$$\bar{\gamma}_k^m = \gamma_k^m - \hat{v}^m(\hat{\theta}_k^m) \quad (34)$$

where $\bar{\gamma}_k^m$ is the corrected filter innovation which will be used in the EKF algorithm at time k , $\gamma_k^m = Z_k^m - \hat{Z}_{k|k-1}^m$ is the filter innovation under the hypothesis H_0^m at time k , $\hat{Z}_{k|k-1}^m$ is the predicted pseudo-range measurement of the m th in-view satellite under the hypothesis H_0^m at time k .

Note that the objective of correcting the filter innovation rather than the pseudo-range measurement itself is to enable the detection of an NLOS MP bias during its whole duration. Finally, an approximate MLRT to detect, estimate and correct the NLOS MP biases is summarized in Algorithm 1.

Algorithm 1. The approximate MLRT to detect, estimate and correct NLOS MP biases in GNSS signals.


```

%Initialization
1:  $\hat{\mathbf{X}}_0 \sim p(\mathbf{X}_0)$ 
2:  $v_i \sim U(v_{\min}, v_{\max})$ 
3:  $\tilde{\omega}_{m,0} = (\tilde{\omega}_{m,0}^1, \dots, \tilde{\omega}_{m,0}^n)$  and  $\tilde{\omega}_{m,0}^i = 1/n$ 
%Time propagation
4: for  $k = 1, \dots, K$  do
%State and measurement prediction in the EKF
5:   Compute  $\hat{\mathbf{X}}_{k|k-1}$  and  $\mathbf{P}_{k|k-1}$  according to (2)
6:   Compute  $\hat{\mathbf{Z}}_{k|k-1}^0 = (\hat{Z}_{1,k|k-1}^0, \dots, \hat{Z}_{N_s,k|k-1}^0)^T$  according to (7)
%Innovation update under different hypotheses
7:    $\gamma_{m,k}^0 = Z_{m,k} - \hat{Z}_{m,k|k-1}^0$ 
8:    $\tilde{\gamma}_{m,k}^i = \gamma_{m,k}^0 - v_i$ 
%Weight prediction and update for bias magnitude samples
9:    $\tilde{\omega}_{m,k|k-1}^i \propto \sum_{i=1}^n \Lambda_i \tilde{\omega}_{m,k-1|k-1}$ 
10:   $\tilde{\omega}_{m,k|k}^i \propto p(\tilde{\gamma}_{m,k}^i | \mathbf{H}_1^m(\theta, v_i)) \tilde{\omega}_{m,k|k-1}^i$ 
% $\Lambda_i$  is the  $i$ th column of the Markov chain transition matrix used in the multiple model algorithm
% $\tilde{\gamma}_{m,k}^i = Z_{m,k} - \hat{Z}_{m,k|k-1}^i$  where  $Z_{m,k}$  and  $\hat{Z}_{m,k|k-1}^i$  are the  $m$ th in-view satellite pseudo-range and
%predicted pseudo-range measurements under the hypothesis  $\mathbf{H}_1^m$  with a bias sampling magnitude
% $v_i$  at time  $k$ 
%MP bias detection, estimation and correction
11:  for  $m = 1, \dots, N_s$  do
12:    Compute  $\tilde{l}_k^m(\theta)$  and  $\varepsilon'$  according to (24) and (36)
13:    Set  $\hat{\theta}_k^m = \arg \max_{\theta} \tilde{l}_k^m(\theta)$  ( $k - L_w < \hat{\theta}_k^m \leq k$ )
14:    if  $\tilde{l}_k^m > \varepsilon'$  a bias is detected
15:      Compute  $\hat{v}^m(\hat{\theta}_k^m)$  according to (31)
16:      Correct the  $m$ th filter innovation according to (34)
17:    end if
18:  end for
%State estimation in the EKF
19:  Compute  $\hat{\mathbf{X}}_{k|k}$  and  $\mathbf{P}_{k|k}$ 
20: end for

```

5. Test threshold analysis

According to the hypothesis testing theory, the MLRT threshold can be determined from the cumulative distribution function of the test statistic under hypothesis H_0 and the significance level α (false alarm rate). Based on the aforementioned derivations, the test statistic $\tilde{l}(\theta)$ of the proposed approximate MLRT in (24) was derived from the test statistic $l(\theta)$ of the MLRT in (19). However, the cumulative distribution functions of the test statistics $l^m(\theta)$ and $\tilde{l}^m(\theta)$ under hypothesis H_0^m have no closed-form expression when the NLOS MP bias has a uniform distribution. Therefore, the empirical cumulative distribution functions of the test statistics $l^m(\theta)$ and $\tilde{l}^m(\theta)$ under hypothesis H_0^m have been computed by Monte Carlo simulations performed using the parameters provided in Table 1. In addition, the state space model defined in Section 2 has been simulated with the parameters

reported in Table 1 and the fault-free GNSS pseudo-range measurements have been computed based on an almanac file including all useful satellite orbit data in the simulations.

The empirical cumulative distribution functions of the test statistics $l^m(\theta)$ and $\tilde{l}^m(\theta)$ under hypothesis H_0^m can be defined as follows:

$$\hat{F}_{l,n_s}(l) = \frac{1}{n_s} \sum_{i=1}^{n_s} I(l_i^m \leq l | H_0^m) \quad (35)$$

and

$$\hat{F}_{\tilde{l},n_s}(l) = \frac{1}{n_s} \sum_{i=1}^{n_s} I(\tilde{l}_i^m \leq l | H_0^m) \quad (36)$$

where I is the indicator function, $(l_1^m, \dots, l_{n_s}^m)$ and $(\tilde{l}_1^m, \dots, \tilde{l}_{n_s}^m)$ are n_s samples of the test statistics $l^m(\theta)$ and $\tilde{l}^m(\theta)$ under hypothesis H_0^m computed by Monte Carlo simulations with a finite window length.

As depicted in Fig. 1, the two empirical cumulative distribution functions (computed with $L_w = 5$) satisfy the relation $\hat{F}_{\hat{l}_{n_s}}(l) > \hat{F}_{\tilde{l}_{n_s}}(l)$. Accordingly, the false alarm rates for the two empirical cumulative distribution functions satisfy $\alpha' \geq \alpha$ when the test threshold is set as the same value for two empirical cumulative distribution functions, where $\alpha = \hat{F}_{\tilde{l}_{n_s}}(l \geq \varepsilon | H_0^m)$ and $\alpha' = \hat{F}_{\hat{l}_{n_s}}(l \geq \varepsilon | H_0^m)$. Thus the false alarm rate α' can be considered as an upper bound for α when the test threshold is given.

The test threshold for the approximate MLRT can be determined by the empirical cumulative distribution functions $\hat{F}_{\hat{l}_{n_s}}(l)$ (which depends on the window length L_w) and the false alarm rate α' . The empirical cumulative distribution functions of the test statistic $\tilde{l}^m(\theta)$ for different window lengths L_w are displayed in Fig. 2. The corresponding thresholds associated with different false alarm rates are given in Table 2. It is clear that the empirical cumulative distribution function decreases as the window length increases. Accordingly, the test threshold is an increasing function of the window length L_w when the false alarm rate α' is given.

6. Algorithm assessment

6.1. Simulation results

6.1.1. Performance measures and test scenarios

In order to evaluate the detection and identification performance of the proposed approximate MLRT approach, the GLRT and to compare it with the approach studied in [31], the following performance measures have been used in this paper:

Table 1
Simulation parameters.

Process noise (velocity)	$\sigma_a = 1 \text{ m/s}^2$
Clock offset noise	$\sigma_b = 3c \times 10^{-10} \text{ m}$
Clock drift noise	$\sigma_d = 2\pi c \times 10^{-10} \text{ m/s}$
GNSS measurement noise	$\sigma_r = 10 \text{ m}$

$c = 3 \times 10^8 \text{ m/s}$ denotes the velocity of light.

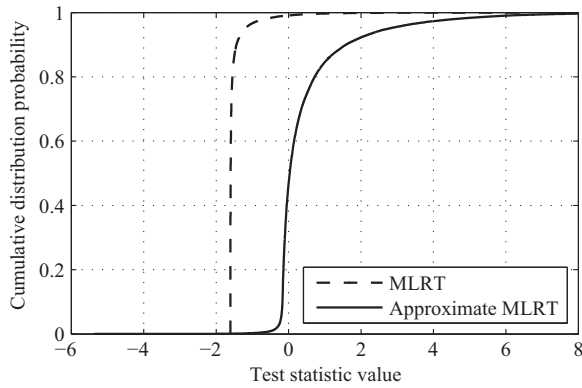


Fig. 1. Empirical cumulative distribution functions of $\hat{F}_{\hat{l}_{n_s}}(l)$ (dashed line) and $\hat{F}_{\tilde{l}_{n_s}}(l)$ (solid line) for a data window length $L_w = 5$.

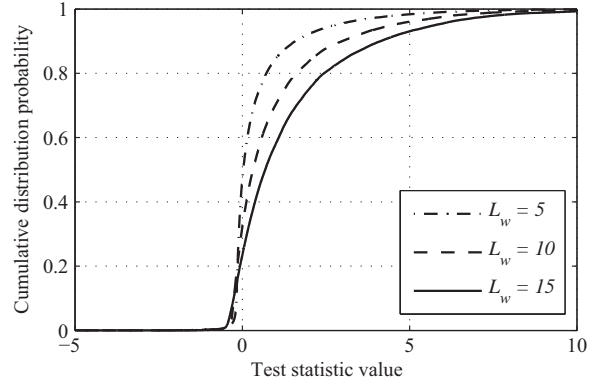


Fig. 2. Empirical cumulative distribution functions associated with different data window lengths.

Table 2
Threshold for different false alarm ratios.

Data window length L_w	False alarm rate		
	0.025	0.05	0.1
5	4.01	2.78	1.62
10	5.83	4.39	2.94
15	7.28	5.62	4.06

- **Average probability of correct detection** (denoted as P_{CD}): A correct detection is obtained when an NLOS MP bias has been detected and a bias is effectively present.
- **Average probability of correct detection and identification** (denoted as P_{CDI}): A correct detection and identification is obtained when an NLOS MP bias has been detected and when the bias sample associated with the largest model probability is the closest to the exact bias magnitude (at a given time).
- **Average probability of correct detection and incorrect identification** (denoted as P_{CDII}): A correct detection and incorrect identification is obtained when an NLOS MP bias has been detected and the bias sample associated with the largest model probability is not closest to the exact bias magnitude (at a given time).
- **Mean detection delay and standard deviation of correct detection** (denoted as $\bar{\tau}$ (s) and σ (s) respectively): A mean detection delay time (s) is obtained by averaging 100 differences between the time instant of the first bias appearance and the time instant of the first bias detection.

In order to evaluate the impact of different numbers of biases on the performance of the approximate MLRT, the multiple model algorithm has been tested with 3, 5 and 7 biases denoted as MLRT(3), MLRT(5) and MLRT(7), for all simulation scenarios. In theory, the pseudo-range MP error can reach magnitudes close to 0.5 of a code chip, i.e., 150 m in the C/A case, depending on the receiver correlation technology [33]. We have assumed in this study that the prior distribution of the MP bias magnitude v is a uniform distribution in the interval $(-75 \text{ m}, 75 \text{ m})$, i.e.,

$p(v) \sim U(-75, 75)$.² The values of the MP bias magnitudes used in our simulations are summarized in Table 3.

Finally, it is assumed that there are 4 in-view satellite pseudo-range measurements during the simulation. In order to reduce the influence of false alarms, the threshold has been set to ensure a false alarm rate of 0.1. The length of the data window is $L_w = 5$ and the filter period equals 1 Hz in all simulations. All algorithms have been coded using MATLAB and run on a laptop with Intel i-7 4710MQ and 8 GB RAM.

6.1.2. Results for single multipath detection

Scenarios with different bias magnitudes have been generated according to the measurement model (7) and 100 Monte Carlo runs.³ In each scenario, an NLOS MP bias with a deterministic magnitude appears on the first pseudo-range measurement (satellite #1) at the 100th second and the bias duration is 20 s.

First, in order to evaluate the influence of Jensen's inequality used in (22) on the detection performances and on the computation load required to compute the test statistic $l(\theta)$ and $\tilde{l}(\theta)$, Table 4 shows the detection results and the execution times for 100 Monte Carlo runs by using the different test statistics with 3 different bias samples. It is clear that the values of P_{CD} for the test statistic $l(\theta)$ and $\tilde{l}(\theta)$ are similar in each scenario. However, the execution time for $\tilde{l}(\theta)$ is much less than that for $l(\theta)$. Thus, without impacting the detection performance, Jensen's inequality can reduce the computation load of the MLRT.

Tables 5 and 6 show the detection performance and the delay measures for the GLRT and the approximate MLRT approaches with different bias samples. The results reported in Table 5 indicate that more than 70% of NLOS MP biases cannot be correctly detected for all approaches when the NLOS MP bias magnitude is less than or close to the measurement noise. The value of P_{CD} gradually increases with the NLOS MP bias magnitude for any detector, as expected. In addition, the value of P_{CD} is larger for the proposed approach than for the GLRT when the bias magnitude is small. This difference between the two detectors gradually disappears as the bias magnitude increases. Due to the competition between too many models in the multiple model, P_{CDII} , significantly increases with the number of models considered in the multiple model for the proposed approximate MLRT.

The results reported in Table 6 indicate that the detection delays for all approaches are decreasing functions of the NLOS MP bias magnitude. The decrease of detection delay for the approximate MLRT is smaller than with the GLRT as the bias magnitude increases. Although the mean detection delay and the standard deviation of the

² The sign of the MP bias magnitude depends on the value of the MP signal carrier phase relative to the LOS signal. When the relative carrier phase $\delta\phi$ is such that $-90^\circ \leq \delta\phi \leq 90^\circ$, the MP signal is referred to as a constructive interference and the LOS signal is strengthened by the MP signals (the sign of the MP bias is positive). Conversely, the MP signal is a destructive interference when the relative carrier phase satisfies the condition $-180^\circ \leq \delta\phi \leq -90^\circ$ or $90^\circ \leq \delta\phi \leq 180^\circ$. In this case, the LOS signal is weakened by the MP signals (the sign of the MP bias is negative).

³ We have observed that the results do not change significantly if we increase the number of Monte Carlo simulations.

Table 3

Bias magnitude samples used for the multiple model algorithm.

	Bias sampling magnitudes (m)						
	1	2	3	4	5	6	7
MLRT(3)	-20	0	20				
MLRT(5)	-30	-20	0	20	30		
MLRT(7)	-35	-25	-15	0	15	25	35

Table 4

Detection performance using the different test statistics.

NLOS MP bias magnitude (m)	$l(\theta)$		$\tilde{l}(\theta)$	
	P_{CD}	Time (s)	P_{CD}	Time (s)
7	0.06	12.0477	0.05	10.9283
12	0.29	12.0416	0.26	10.9405
18	0.55	12.0378	0.62	10.9456
24	0.94	12.0125	0.98	10.9218
28	0.97	12.0239	0.95	11.0296
32	0.97	12.0198	0.97	10.8992

proposed approach are slightly inferior to those of the GLRT, the proposed approach significantly improves the probability of correct detection. Thus the proposed approach provides better bias detection performance than the GLRT for a single NLOS MP.

6.1.3. Results for multiple multipath detection

In order to evaluate the detection performance in the presence of several NLOS MP biases appearing at the same time instant, a second scenario has been generated according to the measurement model (7) as follows:

- The first satellite pseudo-range measurement (satellite #1) is affected by a mean value jump of 28 m during the time interval (40 s, 80 s), and an NLOS MP bias of -26 m appears during the time interval (100 s, 140 s).
- The second satellite pseudo-range measurement (satellite #2) is affected by an NLOS MP bias of 32 m occurring during the time interval (70 s, 150 s).

Since the approach studied in [31] excludes a contaminated measurement after the presence of a mean value jump has been detected, we propose to compare (1) the multiple bias detection performance of the proposed approach with that obtained using the approach of [31] and the GLRT, and (2) the positioning estimation accuracy of the proposed approach with that obtained using the standard EKF, the approach of [31] respectively. 100 Monte Carlo simulations have been run for any scenario. The accurate detection times for multiple NLOS MP (denoted by M) is used to compute the root mean square errors (RMSE) of the estimates defined by $\sqrt{M^{-1} \sum_{i=1}^M (\hat{\mathbf{X}}_k^{(i)} - \mathbf{X}_k)^2}$, where $\hat{\mathbf{X}}_k^{(i)}$ is the i th run result, and $k = 1, \dots, K$ denotes the k th sampling time instant.

The accurate detection times for multiple NLOS MP are depicted in Fig. 3. These results show that the detection

Table 5

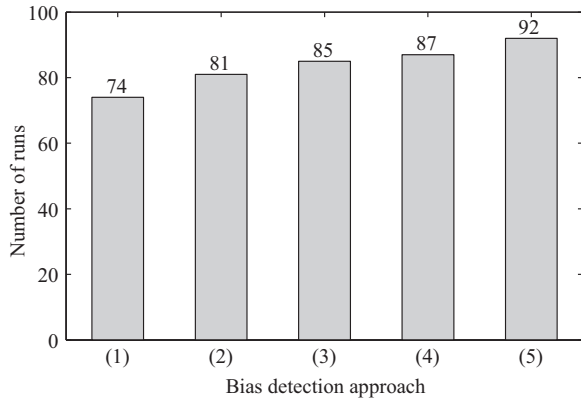
Detection performance for different scenarios.

NLOS MP bias magnitude (m)	MLRT(3)			MLRT(5)			MLRT(7)			GLRT
	P_{CD}	P_{CDI}	P_{CDII}	P_{CD}	P_{CDI}	P_{CDII}	P_{CD}	P_{CDI}	P_{CDII}	P_{CD}
7	0.05	–	–	0.07	–	–	0.10	–	–	0
12	0.26	0.20	0.06	0.30	0.27	0.03	0.24	0.18	0.06	0.14
18	0.62	0.57	0.05	0.59	0.34	0.25	0.74	0.32	0.42	0.40
24	0.98	0.97	0.01	0.90	0.59	0.31	0.94	0.45	0.49	0.61
28	0.95	0.95	0	0.97	0.61	0.36	0.96	0.47	0.49	0.93
32	0.97	0.97	0	0.96	0.50	0.46	0.98	0.47	0.51	0.98

Table 6

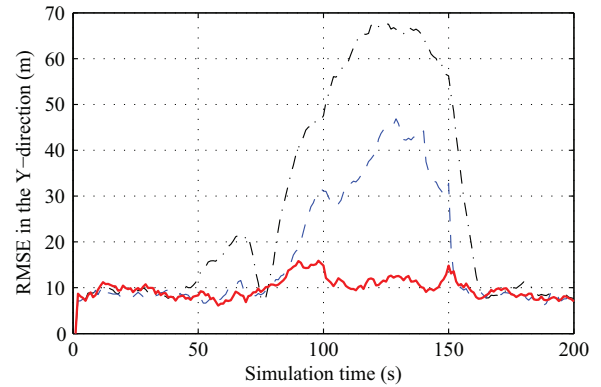
Detection delay for different scenarios.

NLOS MP bias magnitude (m)	MLRT(3)		MLRT(5)		MLRT(7)		GLRT	
	$\bar{\tau}$	σ	$\bar{\tau}$	σ	$\bar{\tau}$	σ	$\bar{\tau}$	σ
7	6.54	–	6.34	–	7.86	–	8.67	–
12	4.23	3.17	4.63	3.04	4.58	3.21	4.75	4.56
18	1.14	2.39	1.27	1.55	1.38	1.79	1.78	3.59
24	–0.66	1.51	–0.94	1.53	–0.86	1.24	1.19	1.79
28	–0.56	1.43	0.76	1.36	–0.80	1.10	0.19	0.87
32	0.52	1.24	–0.71	1.34	–0.78	1.06	0.18	0.71

**Fig. 3.** Accurate detection times for multiple NLOS MP. The bias detection approaches corresponding to the sequence number in the figure are: (1) – GLRT; (2) – Approach in [31]; (3) – MLRT(3); (4) – MLRT(5); (5) – MLRT (7).

performances of the proposed approximate MLRT and the approach studied in [31] are more reliable than for the GLRT due to the prior information considered for the bias magnitude. Moreover, the performance of the approach studied in [31] is close to that of the MLRT(3) and more models in the multiple model algorithm can facilitate the bias detection.

In order to evaluate the effect of different NLOS bias detection approaches on the positioning solution, the RMSEs of the estimated positions with different detection approaches in the Y-direction of the ECEF frame are depicted in Fig. 4. The NLOS MP biases severely impair the positioning solution based on GNSS, as expected. Although the exclusion of contaminated pseudo-range

**Fig. 4.** RMSEs of positioning estimations with different detection approaches. Proposed approach: red solid line; approach in [31]: blue dashed line; standard EKF: black dash-dotted line. (For interpretation of the references to color in this figure caption, the reader is referred to the web version of this paper.)

measurements can partly improve the position accuracy, the accuracy obtained with the MLRT(7) is much better than that obtained with the approach of [31]. This improvement can be explained by the fact that the corrected pseudo-range measurements allow a better system observability.

6.2. Experiment results

6.2.1. Measurement campaign

In this section, the proposed approach is evaluated based on experimental data collected during a measurement campaign carried out in Toulouse center (France). A synchronized integrated navigation system composed of a Novatel receiver coupled to a tactical grade IMAR IMU has been used to provide a reference trajectory. Taking advantage of a ground reference station, differential corrections have been performed to obtain position accuracy close to 1 m for the reference trajectory, which is considered as the ground truth. For assessing the algorithm performance, the vehicle has been equipped with a UBLOX 6T receiver. This receiver delivers not only the position, velocity and time solution, but also, for each satellite, the raw pseudo-range and Doppler frequency measurements, as well as the navigation message. It allows us to compute satellite locations, and to perform timing and propagation correction on the measured pseudo-range. As the aim of the algorithm is to detect and mitigate pseudo-range biases in



Fig. 5. Urban canyon trajectory used in the proposed experiments (obtained with Google Earth).

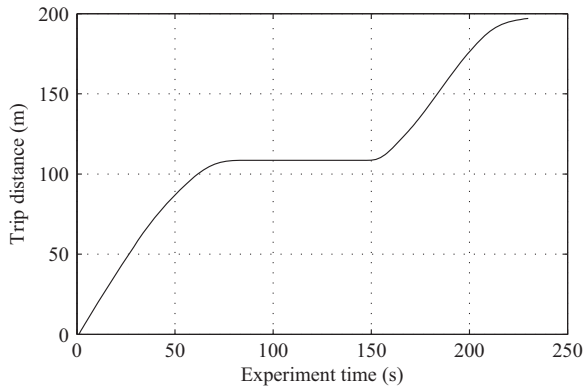


Fig. 6. Trip distance versus time.

the presence of MP, Doppler frequencies that are related to the vehicle velocity are not used here. Data are collected in street urban canyons during which the receiver is strongly affected by MP interferences, and post-processed using Matlab.

Fig. 5 shows the trajectory considered in our measurement campaign (lasting 230 s). Fig. 6 displays the evolution of the trip distance (considered in our experiment) versus time, where the original point is defined as the initial position on the trajectory and the trip distance represents the horizontal distance travelled from the initial position. It is clear that the trip distance does not change during the time interval (71 s, 154 s), as the vehicle is stopped in the middle of two buildings during this period. In this case, the receiver is very sensitive to any MP interference. As it appears at the LOS frequency (the Doppler frequency related to the vehicle velocity is zero), pseudo-range measurements are severely impacted by MP interference during this period.

We propose to compare the positioning estimation accuracy of the MLRT(5) with that obtained using the standard EKF. The in-view satellites observed during the experience are satellites #3, #6, #19, #26, and #27. The standard deviations, which are used to define the process and measurement noises are $\sigma_a = 0.4 \text{ m/s}^2$ and $\sigma_r = 4 \text{ m}$ respectively. The bias sampling magnitudes considered in the multiple model for the MLRT(5) are set as $(-8 \text{ m}, -4 \text{ m}, 0 \text{ m}, 4 \text{ m}, 8 \text{ m})$ in order to make the algorithm sensitive to short-delay MP interferences which characterize urban canyons. Accordingly, we obtain five estimators corresponding to the different bias magnitudes referred to as estimators #1: -8 m ; #2: -4 m ; #3: 0 m ; #4: 4 m ; #5: 8 m . The length of the data window is set to $L_w=5$.

Table 7
Estimated MP appearance times.

In-view satellite	Satellite elevation (deg)	Detected MP appearance time (s)	Bias sample with the largest model probability	
			Experiment time (s)	Sequence index
Satellite #3	81.9–82.4	–	–	–
Satellite #6	77.9–77.5	71–79	71–78	#3
			79–92	#2
			93–97	#1
Satellite #16	56.1–55.5	42–113 127–182	42–46	#3
			47–49	#4
			50–113	#5
			127–129	#5
			130–131 132–182	#4 #5
Satellite #19	60.8–60.3	73–96 99–154	73–78	#3
			79–81	#4
			82–96	#5
			99–154	#5
Satellite #27	82.95–82.92	–	–	–

6.2.2. Results

The results reported in Table 7 indicate the MP appearance time period detected by the MLRT(5). According to the results of the detection algorithm, no MP interference



Fig. 7. Positioning results for different approaches in a urban canyon (obtained with Google Earth). Reference trajectory: white line; proposed approach: red line; standard EKF: blue line. (For interpretation of the references to color in this figure caption, the reader is referred to the web version of this paper.)

impacting pseudo-range measurements has been detected for the satellites #3 and #27. Conversely, the pseudo-range measurements of satellites #6, #16 and #19, which are impacted by the MP interference, are detected by the proposed approach during the same period. The elevation angles of the different in-view satellites are also reported in Table 7. Note that the elevation angles for satellites #3, #6 and #27 are larger than 75° , whereas the elevation angles for satellites #16 and #19 are less than or equal to 60° . The signals from low-elevation-angle satellites, such as satellites #16 and #19, are usually vulnerable to the MP interferences in urban canyons. Conversely, the signals from satellites with high elevation angles, such as satellites #3 and #27, can hardly be impacted by the MP interferences. Accordingly, the detection results for MP appearance coincide with the in-view satellite elevations as reported in Table 7. As mentioned above, five measurement models associated with different bias sampling magnitudes in the multiple model are considered for MLRT(5). The estimators, which correspond to bias sampling magnitudes with the largest model probability for the detected time intervals, are indicated in Table 7. Since the magnitude of the MP interferences changes for different time instants, the magnitude of the bias sample

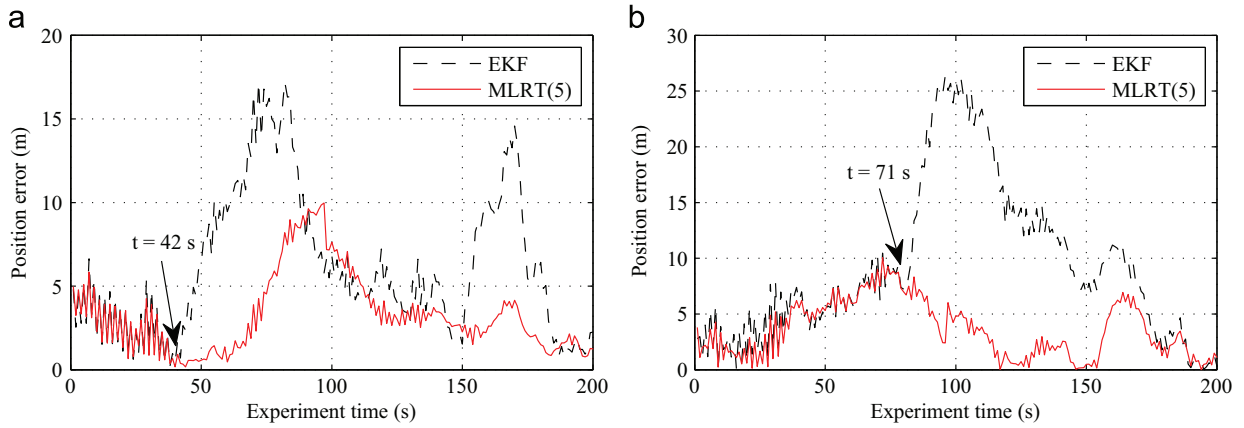


Fig. 8. Positioning errors versus time. (a) Horizontal error. (b) Vertical error.

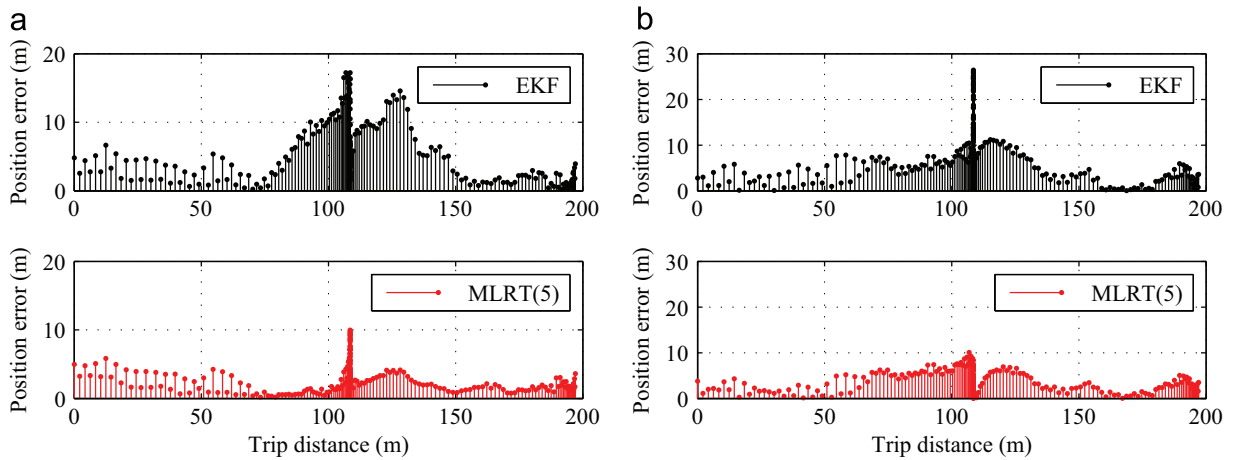


Fig. 9. Positioning errors versus trip distance. (a) Horizontal error. (b) Vertical error.

associated with the largest model probability also changes with time.

Figs. 7 and 8 display the positioning results (illustrated with Google Earth) and the corresponding positioning errors (the horizontal and vertical errors versus time) for the different approaches. It is clear that MP interferences severely impair the positioning solution if these interferences are not processed within the receiver. As shown in Fig. 8 the time instances, from which the horizontal and vertical positioning errors based on the standard EKF start to deteriorate, coincide with the MP appearance time determined by the proposed approach. Conversely, the positioning errors obtained with the proposed approach remains lower than 10 m, confirming that the MP interferences appearing on the pseudo-range measurements have been detected and mitigated.

Fig. 9 displays the horizontal and vertical errors versus the trip distance. It is clear that the positioning accuracy, especially in the vertical direction, is sensitive to the MP interferences when the vehicle stops in the middle of two buildings. As a consequence, the impact resulting from the MP interference error is the maximum during this period. However, the proposed approach can effectively mitigate the impact of the MP interference in this case. Increasing the duration of the observation window depending on the vehicle dynamic could also facilitate MP detection when the vehicle remains at the same location.

7. Conclusion

This paper proposed an approximated marginalized likelihood ratio test based on Jensen's inequality to detect, identify and estimate the NLOS multipath biases affecting GNSS pseudo-range measurements in urban canyons. The effects of NLOS multipath interferences were modeled as mean value jumps. The proposed approach was based on a marginalized likelihood ratio test approximated using a Monte Carlo integration and Jensen's inequality. The multiple model algorithm was introduced to update the prior information of each bias magnitude sample in order to improve its detection. A simulation study was implemented in order to compare the performance of the proposed approach with the GLRT and the approach studied in [31]. Although the mean detection delay and the standard deviation of the proposed approach were slightly inferior to those of the GLRT, the probability of correct detection increases significantly (when compared to the GLRT) due to the introduction of a prior information about the bias magnitude. A comparison with the standard EKF and the approach studied in [31] showed that the positioning accuracy was improved by the proposed approach. Finally, the proposed approach was validated by processing data collected from a measurement campaign carried out in an urban environment. The proposed approach proved its efficiency for MP interference detection and mitigation, resulting in improving positioning accuracy.

Considering that more accurate state models facilitate the NLOS MP bias detection and that inertial measurement units (IMU) can provide more reliable information about the dynamic of the vehicle, our future work will be devoted to implement the proposed approach within an

IMU/GNSS integration. It would also be interesting to allow the length of the observation window to adapt dynamically depending on the receiver motion (especially when the receivers stop and do not move anymore). Finally the application of the proposed approach for other applications, such as mobile phone communication in urban environments, would deserve some attention.

Acknowledgments

This research was supported by the National Natural Science Foundation of China (#61473230, #61135001). We also thank the anonymous reviewers for their valuable suggestions, which helped to improve the quality of the paper.

References

- [1] E. Kaplan, C. Hegarty, *Understanding GPS: Principles and Applications*, 2nd edition, Artech House, Norwood, MA, 2006.
- [2] L.Y. Liu, M.G. Amin, Tracking performance and average error analysis of GPS discriminators in multipath, *Signal Process.* 89 (6) (2009) 1224–1239.
- [3] Z.Y. Jiang, P.D. Groves, NLOS-GPS signal detection using a dual-polarisation antenna, *GPS Solut.* 18 (1) (2014) 15–26.
- [4] S. Daneshmand, A. Broumandan, N. Sokhandan, G. Lachapelle, GNSS multipath mitigation with a moving antenna array, *IEEE Trans. Aerosp. Electron. Syst.* 49 (1) (2013) 693–698.
- [5] A.J. van Dierendonck, P.C. Fenton, T. Ford, Theory and performance of narrow correlator spacing in a GPS receiver, *J. Navig.* 39 (3) (1992) 265–283.
- [6] L. Garin, F. van Diggelen, J.M. Rousseau, Strobe & Edge correlator multipath mitigation for code, in: Proceedings of the 9th International Technical Meeting of the Satellite Division of the Institute of Navigation (IONGPS 1996), Kansas City, MO, USA, 1996, pp. 657–664.
- [7] B.R. Townsend, P.C. Fenton, A practice approach to the reduction of pseudorange multipath error in a L1 gps receiver, in: Proceedings of the 7th International Technical Meeting of the Satellite Division of the Institute of Navigation (IONGPS 1994), Salt Lake City, UT, USA, 1994, pp. 143–148.
- [8] G.A. McGraw, M.S. Braasch, GNSS multipath mitigation using gated and high resolution correlator concepts, in: Proceedings of the National Technical Meeting of the Institute of Navigation (IONNTM 1999), San Diego, CA, USA, 1999, pp. 333–342.
- [9] N. Jardak, A. Vervisch-Picois, N. Samama, Multipath insensitive delay lock loop in GNSS receivers, *IEEE Trans. Aerosp. Electron. Syst.* 47 (4) (2011) 2590–2609.
- [10] R.D.J. van Nee, J. Siereveld, P.C. Fenton, B.R. Townsend, The multipath estimating delay lock loop: approaching theoretical accuracy limits, in: Proceedings of 1994 IEEE Position, Location and Navigation Symposium (PLAN 1994), Las Vegas, NV, USA, 1994, pp. 246–251.
- [11] L.L. Weill, Multipath mitigation: How good can it get with new signals? *GPS World* (June) (2003) 106–113.
- [12] M. Sahnoudi, M.G. Amin, Fast iterative maximum-likelihood algorithm (fimla) for multipath mitigation in the next generation of GNSS receivers, *IEEE Trans. Wireless Commun.* 7 (11) (2008) 4362–4374.
- [13] M. Sahnoudi, M.G. Amin, Robust tracking of weak GPS signals in multipath and jamming environments, *Signal Process.* 89 (7) (2009) 1320–1333.
- [14] N. Blanco-Delgado, F.D. Nunes, Multipath estimation in multicorrelator GNSS receivers using the maximum likelihood principle, *IEEE Trans. Aerosp. Electron. Syst.* 48 (4) (2012) 3222–3233.
- [15] S.F.S. Dardin, V. Calmettes, B. Priot, J.-Y. Tournet, Design of an adaptive vector-tracking loop for reliable positioning in harsh environment, in: Proceedings of the 26th International Technical Meeting of the Satellite Division of the Institute of Navigation (IONGNSS 2013), Nashville, TN, USA, 2013, pp. 3548–3559.
- [16] M. Spangenberg, A. Giremus, P. Poire, J.-Y. Tournet, Multipath estimation in the global positioning system for multicorrelator receivers, in: Proceedings of the 32th IEEE International Conference on Acoustics, Speech and Signal Processing (ICASSP 2007), Honolulu, HI, USA, 2007, pp. 1277–1280.

- [17] P. Closas, C. Fernandez-Prades, J.A. Fernandez-Rubio, A Bayesian approach to multipath mitigation in GNSS receivers, *IEEE J. Sel. Top. Signal Process.* 3 (4) (2009) 695–706.
- [18] V. Pereira, A. Giremus, E. Grivel, A Boltzmann machine to model the multipath environment for particle filtering based GPS navigation, in: *Proceedings of the 20th European Signal Processing Conference (EUSIPCO 2012)*, Bucharest, Romania, 2012, pp. 185–189.
- [19] P.D. Groves, Shadow matching: a new GNSS positioning technique for urban canyons, *J. Navig.* 64 (3) (2011) 417–430.
- [20] A. Bourdeau, M. Sahnoudi, J.-Y. Tournet, Constructive use of GNSS NLOS-multipath: augmenting the navigation Kalman filter with a 3D model of the environment, in: *Proceedings of the 15th International Conference on Information Fusion (FUSION 2012)*, Singapore, 2012, pp. 2271–2276.
- [21] D.E. Gustafson, J.M. Elwell, J.A. Soltz, Innovative indoor geolocation using RF multipath diversity, in: *Proceedings of 2006 IEEE/ION Position, Location and Navigation Symposium (PLAN 2006)*, San Diego, CA, USA, 2006, pp. 904–912.
- [22] S.G. Razul, C.-H. Lim, C.M.S. See, Bayesian method for NLOS mitigation in single moving sensor Geo-location, *Signal Process.* 91 (7) (2011) 1613–1621.
- [23] M. Spangenberg, V. Calmettes, O. Julien, J.-Y. Tournet, G. Duchateau, Detection of variance changes and mean value jumps in measurement noise for multipath mitigation in urban navigation, *J. Navig.* 57 (1) (2010) 35–52.
- [24] N. Viandier, D.F. Nahimana, J. Marais, E. Duflos, GNSS performance enhancement in urban environment based on pseudo-range error model, in: *Proceedings of 2008 IEEE/ION Position, Location and Navigation Symposium (PLAN 2008)*, Monterey, CA, USA, 2008, pp. 337–382.
- [25] A. Giremus, J.-Y. Tournet, V. Calmettes, A particle filtering approach for joint detection/estimation of multipath effects on GPS measurements, *IEEE Trans. Signal Process.* 55 (4) (2007) 1275–1285.
- [26] S.M. Kay, *Fundamentals of Statistical Signal Processing, Volume II: Detection Theory*, Prentice Hall, Upper Saddle River, NJ, 2001.
- [27] A.S. Willsky, H.L. Jones, A generalized likelihood ratio approach to the detection and estimation of jumps in linear systems, *IEEE Trans. Autom. Control* 21 (1) (1976) 108–112.
- [28] F. Gustafsson, The marginalized likelihood ratio test for detecting abrupt changes, *IEEE Trans. Autom. Control* 41 (1) (1996) 66–78.
- [29] D.A. dos Santos, T. Yoneyama, A Bayesian solution to the multiple composite hypothesis testing for fault diagnosis in dynamic systems, *Automatica* 47 (1) (2011) 158–163.
- [30] F. Kiasi, J. Prakash, S. Patwardhan, S.L. Shah, A unified framework for fault detection and isolation of sensor and actuator biases in linear time invariant systems using marginalized likelihood ratio test with uniform priors, *J. Process Control* 23 (9) (2013) 1350–1361.
- [31] A. Giremus, J. Grolleau, An unscented Kalman filter based maximum likelihood ratio for NLOS bias detection in UMTS localization, in: *Proceedings of the 16th European Signal Processing Conference (EUSIPCO 2008)*, Lausanne, Switzerland, 2008, pp. 1–5.
- [32] P.D. Groves, *Principles of GNSS, Inertial and Multisensor Integrated Navigation Systems*, Artech House, London, 2008.
- [33] P. Misra, P. Enge, *Global Positioning System: Signals, Measurements and Performance*, Ganga-Jamuna Press, Lincoln, MA, 2001.
- [34] D.J.C. MacKay, *Information Theory, Inference and Learning Algorithms*, Cambridge University Press, Cambridge, 2003.
- [35] Y. Bar-Shalom, X.R. Li, T. Kirubarajan, *Estimation with Applications to Tracking and Navigation: Theory Algorithms and Software*, John Wiley & Sons, 2004.